*Chinese Journal of*
**POLYMER SCIENCE**

RESEARCH ARTICLE

https://doi.org/10.1007/s10118-022-2676-6
*Chinese J. Polym. Sci.* **2022**, *40*, 338–344

# Morphology Engineering for Covalent Organic Frameworks (COFs) by Surfactant Mediation and Acid Adjustment

Guang-Hui Yang, Zhe Zhang*, Cong-Cong Yin, Xian-Song Shi, and Yong Wang*

*State Key Laboratory of Materials-Oriented Chemical Engineering, College of Chemical Engineering, Nanjing Tech University, Nanjing 211816, China*

Electronic Supplementary Information

**Abstract** Two-dimensional covalent organic frameworks (COFs) with specific morphologies including nanofibers and nanoplates are highly desired in both nanoscience research and practical applications. Thus far, however, morphology engineering for COFs remains challenging because the mechanism underlying the morphology formation and evolution of COFs is not well understood. Herein, we propose a strategy of surfactant mediation coupled with acid adjustment to engineer the morphology of a $\beta$-ketoenamine-linked COF, TpPa, during solvothermal synthesis. The surfactants function as stabilizers that can encapsulate monomers and prepolymers to create micelles, enabling the formation of fiber-like and plate-like morphologies of TpPa rather than irregularly shaped aggregates. It is also found that acetic acid is important in regulating such morphologies, as the amino groups inside the prepolymers can be precisely protonated by acid adjustment, leading to an inhibited ripening process for the creation of specific morphologies. Benefitting from the synergistic enhancement of surfactant mediation and acid adjustment, TpPa nanofibers with a diameter down to ~20 nm along with a length of up to a few microns and TpPa nanoplates with a thickness of ~18 nm are created. Our work sheds light on the mechanism underlying the morphology formation and evolution of TpPa, providing some guidance for exquisite control over the growth of COFs, which is of great significance for their practical applications.

**Keywords** Covalent organic frameworks (COFs); Morphology engineering; Surfactants; Nanofibers; Nanoplates

**Citation:** Yang, G. H.; Zhang, Z.; Yin, C. C.; Shi, X. S.; Wang, Y. Morphology engineering for covalent organic frameworks (COFs) by surfactant mediation and acid adjustment. *Chinese J. Polym. Sci.* **2022**, *40*, 338–344.

## INTRODUCTION

Two-dimensional (2D) covalent organic frameworks (COFs), an eminent representative of crystalline and porous materials, featuring shape-persistent nanoporosities, large surface areas, entirely organic backbones, and readily customized functionalities, are finding enormous applications in energy harvesting, environmental remediation, industrial catalysis, and chemical separation.[1–5] COFs are created following the principle of reticular chemistry, in which topologically structured building blocks are covalently bonded, yielding extended structures with strict periodicity and long-range regularity.[6–8] Solvothermal synthesis is widely recognized as a general synthetic protocol for producing COFs.[9–11] The reaction is typically conducted in sealed vessels that provide desired atmospheres for reaction reversibility, which is beneficial for crystallization and enables creating COFs with high crystallinity, large surface area and well-defined porosity.[12–14] During the solvothermal procedure, a large number of crystal nuclei are rapidly generated once the building blocks (starting monomers) contact and mix with each other due to their inherently fast reaction kinetics. Thus, massive crystal nuclei would continue to grow in an anisotropic fashion, ultimately ripening into polycrystalline architectures with irregular shapes and morphologies.[15,16] For practical applications, however, COFs with specific morphologies such as fibers, plates and spheres are being increasingly sought because well-defined microstructures would endow COFs with unique functionalities more suitable for structure-performance enhancement in various applications.[17–22] To this end, several efforts have suggested that by leveraging the behaviors in either thermodynamics or kinetics during the nucleation-growth of COFs, the morphology of COFs would be significantly influenced.[12,21,23] Considering that the thermodynamics and kinetics can be regulated by the synthesis parameters during the solvothermal reaction, specific morphologies can be generated by rationally optimizing the type, dosage and ratio of solvents, catalysts and additives.[15,16] For instance, a fiber-like morphology was effectively created in the presence of excess polar solvents including water and alcohols, which is thought to be driven by the dissolution-recrystallization process.[24–26] However, it remains a great challenge to regulate the morphology of COFs along the solvothermal route in a controllable manner, and the mechanism underlying the formation and evolution of the specific morphologies is far from fully understood.

* Corresponding authors, E-mail: zhangzhe@njtech.edu.cn (Z.Z.)
E-mail: yongwang@njtech.edu.cn (Y.W.)

Received November 2, 2021; Accepted November 30, 2021; Published online January 20, 2022

© Chinese Chemical Society
Institute of Chemistry, Chinese Academy of Sciences

Surfactants have shown great potential in regulating the morphologies of various nanomaterials including silica,[27,28] metal-organic frameworks (MOFs),[29,30] and COFs.[31,32] By virtue of their amphiphilic molecular structure, surfactants are prone to form micelles in aqueous solution with buried hydrophobic chains and exposed hydrophilic chains.[32–34] Therefore, surfactants can be regarded as mediators that not only function as soft templates to form specific morphologies but also serve as stabilizers to relieve the agglomeration of nanomaterials. Very recently, Puigmartí-Luis and coworkers reported an innovative strategy by using a surfactant pair (a mixture of both cationic and anionic surfactants) to prepare sub-20-nm-sized colloidal COFs in water.[35] The cationic surfactant, hexadecyltrimethylammonium bromide (CTAB), and the anionic surfactant, sodium dodecyl sulfate (SDS), co-form a micellar medium that provides exquisite control over the growth of COF crystallites. Therefore, we envision such a surfactant pair functioning as a viable mediator that could controllably regulate the morphology of COFs.

Inspired by this method, herein, we proposed a strategy of surfactant mediation coupled with acid adjustment to engineer the morphology formation and evolution of a $\beta$-ketoenamine-linked COF, TpPa, during solvothermal synthesis (Scheme 1). The surfactant pair composed of CTAB and SDS were employed to generate micelles for encapsulating monomers and prepolymers, enabling the formation of COFs with fiber/plate-like morphologies. It is obviously different from the previous report of surfactant assisted synthesis of sub-20-nm-sized COF particles.[35] We also found that adjusting the amount of acetic acid to endow the amino groups with precise protonation is of vital importance in the formation and evolution of nanofibers and nanoplates. This work systematically studied the formation and evolution of fiber/plate-like morphologies by leveraging surfactant mediation and acetic acid adjustment under solvothermal conditions, providing some guidance on precise control over the growth of COFs.

## EXPERIMENTAL

### Materials

1,3,5-Triformylphloroglucinol (Tp, 95%) was supplied by Jilin Chinese Academy of Sciences-Yanshen Technology Co., Ltd. *p*-Phenylenediamine (Pa, 97%), CTAB (99%), SDS (98.5%), and 1,4-dioxane (99%) were purchased from Shanghai Aladdin Biochemical Technology Co., Ltd. Acetic acid (99.5%), ammonia water (25%~28%) and ethanol were obtained from Sinopharm Chemical Reagent Co., Ltd. All chemicals were used as received unless otherwise indicated. Silicon wafers and poly(ether sulfone) (PES, mean pore size, 0.22 μm) macroporous membranes were used as the substrate for the microscopy imaging of COFs. Deionized water (conductivity <10 μS·cm$^{-1}$) was used in all experiments.

### Synthesis of TpPa

To prepare the Tp solution, Tp (0.1 mmol) was first dispersed in 250 μL of 1,4-dioxane and then added to 45 mL of CTAB (0.1 mol/L) aqueous solution followed by ultrasonic treatment. Next, 3.4 mL of SDS (0.1 mol/L) aqueous solution was added. The Pa solution was prepared by the same procedure as that for the Tp solution. The two precursor solutions were mixed together and charged into thick-walled glass tubes, after which acetic acid in various amounts (0.01, 0.1, 1, 3, 5, 10 mL) was added. The tube

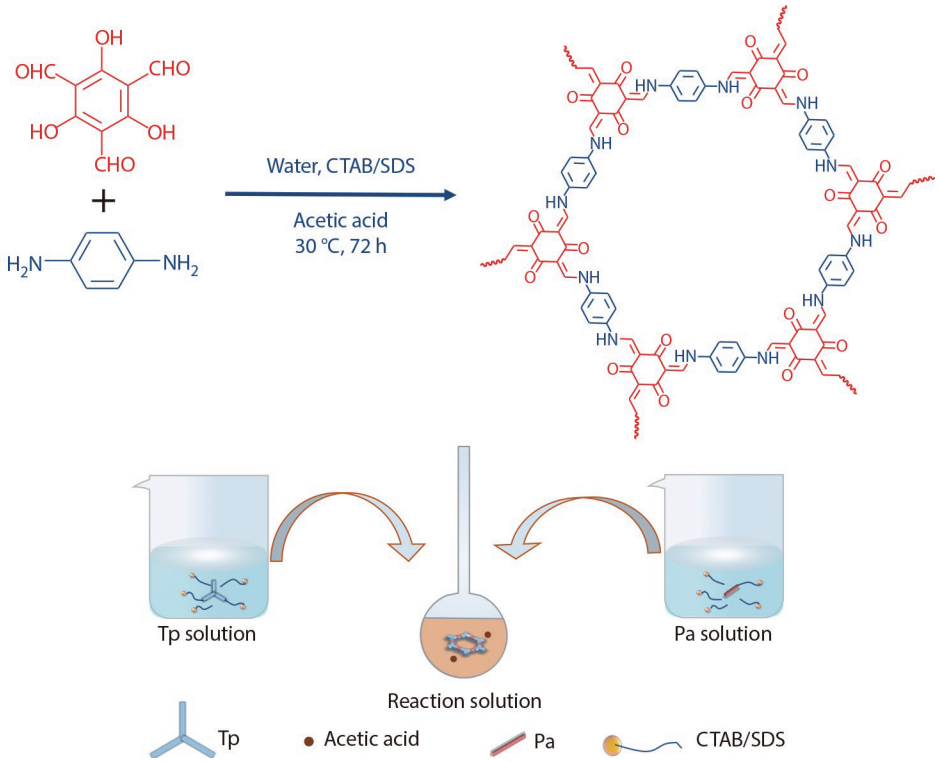


**Scheme 1** Schematic presentation of the preparation of TpPa with different morphologies.

https://doi.org/10.1007/s10118-022-2676-6

was frozen in liquid nitrogen, subjected to three freeze-pump-thaw cycles, and then sealed under vacuum. The sealed tube was placed in a thermostated water bath at 30 °C for 72 h. After the reaction, the acidic mixtures were neutralized by ammonia water at an amount equal to that of acetic acid. Then, the mixtures were demulsified by 100 mL of ethanol, yielding reddish-brown precipitates. The precipitates were further filtered, washed with excess ethanol and water, and vacuum-dried at 70 °C for 24 h.

### Characterizations

The chemical compositions of the COFs were analyzed by Fourier transform infrared (FTIR) spectroscopy (Nicolet 8700, Thermo Fisher Scientific). Morphological images of the COFs were captured on a field-emission scanning electron microscopy (SEM) system (S-4800, Hitachi) operating at 3.0 kV. Prior to imaging, samples were coated with an ultrathin layer of gold on an MC1000 ion-sputtering apparatus. X-ray diffraction (XRD) patterns of the COFs were collected on a Smart Lab X-ray diffractometer (Rigaku Corporation) at $2\theta$ of 2°–30° with a step of 0.02(°)·$s^{-1}$. High-resolution transmission electron microscopy (HRTEM) images were obtained on a JEM-2100 microscope (JEOL) operating at 200 kV. Samples were prepared by drop-casting COF dispersions on copper grids followed by solvent evaporation. Atomic force microscopy (AFM) images were collected on an XE-100 imaging system (Park Systems). The scanning rate was 0.5 Hz. Nitrogen adsorption-desorption isotherms of COFs were collected on a surface area and porosimetry system (ASAP2460, Micromeritics). Brunauer-Emmett-Teller (BET) analyses were adopted to determine the surface areas. The pore width distributions were obtained by nonlocal density functional theory (NLDFT). The pH value of aqueous samples was adjusted according to a pH meter (FE28, Mettler Toledo).

## RESULTS AND DISCUSSION

In this work, a $\beta$-ketoenamine-linked COF, TpPa, was selected as the paradigm for the investigation of morphology formation and evolution, owing to its excellent thermal/chemical stabilities, which hold great promise in various practical applications.[36–39] We noticed that the presence of surfactants and acetic acid significantly influenced the formation of the specific morphology of TpPa in the solvothermal synthesis. Thus, surfactants and acetic acid were adopted as the main synthesis parameters to investigate the effects of such parameters on the morphology formation and evolution. The solvothermal synthesis was conducted in aqueous solutions with a small amount of 1,4-dioxane working as the cosolvent to dissolve the monomers. In the absence of surfactants and acetic acid, TpPa was obtained as large aggregates composed of irregularly shaped fibers fused together (Fig. 1a). When acetic acid (5 mL) was introduced into the synthesis system, well-defined fibers along with particles were formed (Fig. 1b). However, TpPa was still obtained as large aggregates. With the surfactant pair containing SDS (anionic surfactant) and CTAB (cationic surfactant) individually added into the synthesis system, interestingly, the fiber-like structures disappeared, and small particles emerged (Fig. 1c). In this case, large aggregates were not formed, mainly because the surfactants could function as stabilizers to provide excellent dispersion for TpPa.

To verify the roles of surfactants and acetic acid in the formation of specific morphologies, these reagents were simultaneously introduced into the synthesis system. When the surfactants and acetic acid were both added, TpPa with specific morphologies, that is, nanofibers and nanoplates, was formed (Figs. 2a–2f). Thus, this result indicates that the presence of both surfactants and acetic acid significantly influences the morphology formation of TpPa.

We further investigated the effects of acetic acid on the

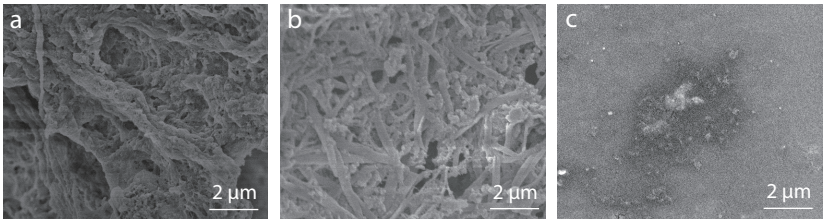


**Fig. 1** SEM images of TpPa synthesized under different conditions: (a) without surfactants and acetic acid, (b) with acetic acid only, (c) with surfactants only.

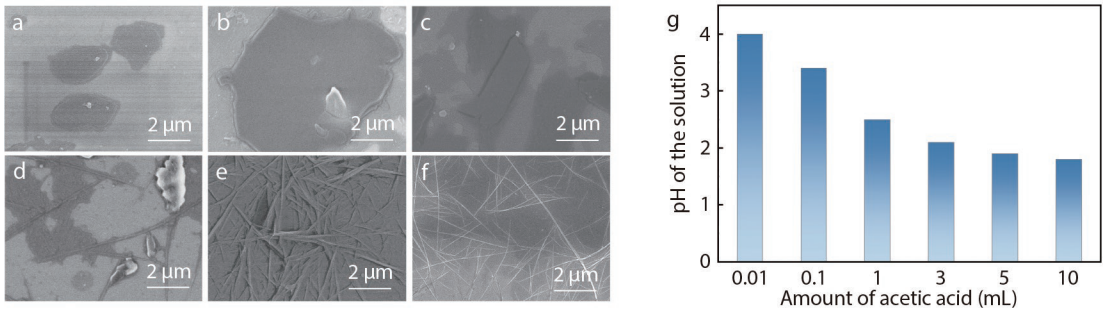


**Fig. 2** Effects of acetic acid on morphology formation and evolution under the mediation of surfactants. SEM images of TpPa formed with different amounts of acetic acid: (a) 0.01 mL, (b) 0.1 mL, (c) 1 mL, (d) 3 mL, (e) 5 mL, and (f) 10 mL. (g) The pH values of aqueous solutions corresponding to different amounts of acetic acid.

https://doi.org/10.1007/s10118-022-2676-6

morphology evolution under the mediation of surfactants. The pH values of aqueous solutions were measured as 4.0, 3.4, 2.5, 2.1, 1.9 and 1.8, corresponding to acetic acid amounts of 0.01, 0.1, 1, 3, 5 and 10 mL, respectively (Fig. 2g). When the pH values of the aqueous solutions decreased from 4.0 to 2.5, TpPa exhibited a plate-like morphology with a planar size of up to a few microns (Figs. 2a–2c). As the pH value decreased to 2.1, the plate-like structures coupled with the fiber-like morphologies were formed (Fig. 2d). As the pH values continuously decreased to 1.9 and 1.8, the plate-like morphology disappeared, while a fiber-like morphology appeared (Figs. 2e and 2f). Therefore, the above results clearly indicated that the addition of acetic acid into the synthesis system together with mediation by the surfactants effectively created TpPa with plate-like and fiber-like morphologies. Alternatively, plate-like and fiber-like morphologies could be precisely and continuously tuned by adjusting the pH values (by acetic acid) during surfactant-mediated synthesis.

Aspects of the microstructures including the porosity properties, crystalline characteristics and height profiles of TpPa nanofibers and nanoplates were further characterized. TpPa nanoplates (in ~85% yield) and nanofibers (in ~78% yield) formed at pH values of 2.5 and 1.8, respectively, were adopted in these investigations. The nitrogen adsorption-desorption isotherms of TpPa nanofibers and nanoplates are shown in Fig. 3(a), and both exhibited the typical Type-I isotherm curve with fast adsorption kinetics at low relative pressure, indicative of microporous characteristics. The BET surface areas of the TpPa nanofibers and nanoplates were calculated to be 322.1 and 72.8 $m^2 \cdot g^{-1}$, respectively. In addition, based on the NLDFT model, the pore widths of TpPa nanofibers and nanoplates were calculated to be 1.42 and 1.34 nm, respectively. Notably, the surface area of TpPa nanoplates is lower than that of TpPa nanofibers, suggesting the relatively low nanoporosity of TpPa nanoplates. The reason is probably that the nanopores of TpPa nanoplates could be partially blocked during the synthesis, which will be discussed later. The crystalline characteristics of TpPa nanofibers and nanoplates were analyzed by HRTEM imaging. The HRTEM, fast Fourier transform (FFT) and inverse fast Fourier transform (IFFT) images of TpPa nanoplates and nanofibers are shown in Figs. 3(c) and 3(d), respectively. The clearly observed lattice fringes confirmed that both TpPa nanofibers and nanoplates were crystalline. Besides, XRD patterns of TpPa nanofibers and nanoparticles exhibit distinct peaks at ~4.7°, corresponding to the (100) crystallographic plane (Fig. S1 in the electronic supplementary information, ESI). Broad peaks also emerge at ~27°, which corresponds to the (001) plane. This provides evidence for the synthesis of TpPa nanofibers and nanoparticles with periodic structures. Moreover, the height profiles of TpPa nanofibers and nanoplates were measured by AFM (Figs. 3e and 3f). The thickness of the TpPa nanoplates was ~18 nm, while the diameter of the TpPa nanofibers was ~20 nm. The TpPa nanoplates were observed to be relatively thick, while the TpPa nanofibers had a high length-diameter ratio. In addition, the chemical compositions of the nanoplates and nanofibers were characterized. FTIR spectra confirmed the formation of a $\beta$-ketoenamine linkage, as the characteristic bands of C=C and C—N bonds at 1580 and 1256 $cm^{-1}$ appeared, respectively (Fig. S2 in ESI). These typical peaks matched well with those of TpPa reported in previous work,[36,40] evidencing the successful synthesis of TpPa.

To gain insight into the evolution mechanism of TpPa nanofibers and nanoplates, a time-dependent SEM imaging method was adopted to probe the nucleation-growth process. The pH values for the synthesis of TpPa nanoplates and nanofibers were 2.5 and 1.8, respectively. We first checked the appearance of the reaction solutions at reaction durations of 0, 0.5, 1 and 72 h. As the reaction proceeded to 72 h, the colors of both types of reaction solutions gradually darkened, implying continuous reactions (Fig. S3 in ESI). To perform SEM imaging, the reaction solutions formed from various reaction durations were then subjected to vacuum filtration using PES macroporous substrates, causing TpPa to deposit on their flat surfaces. For the TpPa nanofibers, when monomer solutions began to contact, a large number of short fibers featuring a

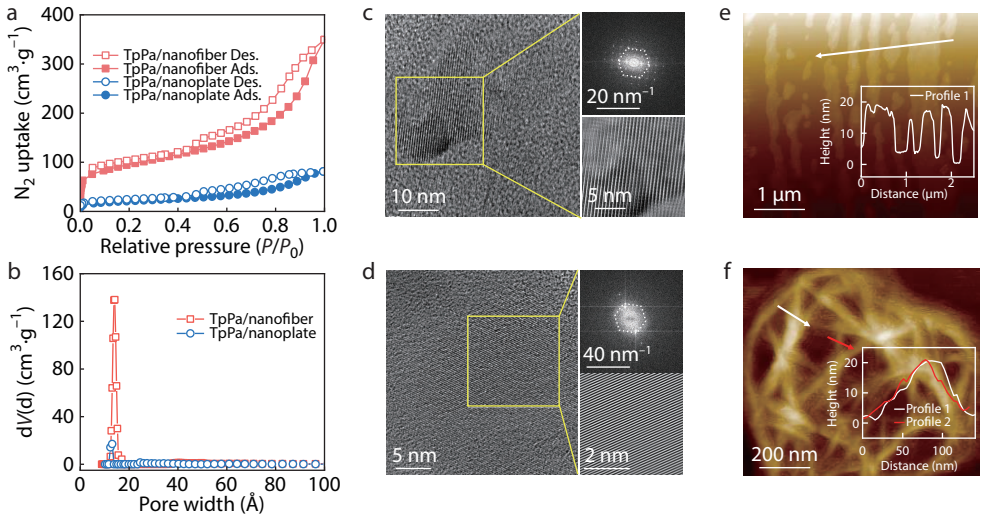


**Fig. 3** Characterizations of TpPa nanoplates and nanofibers. Nitrogen adsorption-desorption isotherms (a) and pore width distributions (b) of TpPa nanoplates and nanofibers; (c) HRTEM image of TpPa nanoplate with FFT (top-right) and IFFT images (bottom-right); (d) HRTEM image of TpPa nanofiber with FFT (top-right) and IFFT images (bottom-right); (e) AFM image of TpPa nanoplates (inset shows the corresponding height profile); (f) AFM image of TpPa nanofibers (inset shows corresponding height profiles).

https://doi.org/10.1007/s10118-022-2676-6

low length-diameter ratio were rapidly formed (Fig. 4a). As the synthesis duration increased to 0.5 and 1 h, the length of the fibers became longer (Figs. 4b and 4c). Finally, as the synthesis duration was prolonged to 72 h, distinct long fibers with a high length-diameter ratio were formed, which is consistent with the morphology observed by SEM and AFM analysis (Fig. 4d). For the TpPa nanoplates, small plates along with short fibers appeared once the monomer solutions were mixed together (Fig. 4e). When the synthesis duration reached 0.5 h, except for the small plates (not shown herein), massive short fibers were formed (Fig. 4f). As the synthesis duration proceeded to 1 h, remarkably, plate-like structures with a large number of fibers fused together emerged (Fig. 4g). Ultimately, when the synthesis duration was prolonged to 72 h, a plate with a planar size of up to a few microns was formed (Fig. 4h). The above results demonstrated a continuous and dynamic morphology evolution process of TpPa nanofibers and nanoplates.

Overall, on the basis of the aforementioned results, we understand the morphology formation and evolution of TpPa nanofibers and nanoplates in the presence of acetic acid under the mediation of these surfactants. For morphology formation, surfactants play two important roles in the synthesis of TpPa.[32,34] The first role is to act as a dispersion stabilizer. The hydrophobic chains of the surfactants were enriched on the surface of the monomer and the prepolymers, driven by noncovalent interactions. However, the hydrophilic chains were aligned outside the monomer and the prepolymers toward the aqueous solutions, preventing them from agglomeration. The other role is to slow down the growth kinetics of TpPa nuclei on the spatial-temporal scale compared to the case without surfactants. The surfactants enabled micellar encapsulation of monomers and prepolymers to slow the growth kinetics instead of direct and fast amine-aldehyde condensation, capable of controlling the growth of TpPa. Therefore, when the surfactants were absent, the monomers would rapidly react with each other and further polymerize into a large number of small crystal nuclei, thus ripening into large aggregates. When surfactants were added, these molecules wrapped monomers and prepolymers to form dispersed micelles, slowing the reaction kinetics. In addition, acetic acid is indispensable in providing specific morphologies because it also functions as a catalyst for the synthesis of COFs.[11] The catalyst facilitated the formation of highly crystalline COFs rather than amorphous forms.[41,42] Thus, ultimately, when surfactants and acetic acid were added to the reaction system simultaneously, TpPa with fiber-like or plate-like morphologies could be effectively prepared (Fig. 5).

Regarding the morphology evolution, under the mediation of surfactants, the amount of acetic acid was adjusted to vary the pH value of the reaction solutions, enabling precise control over the protonation of amine monomers. Protonation of amine monomers would reduce their reactivity with aldehyde monomers, because the protonated amino groups of the amine monomers are not capable of effective nucleophilic attack to the carbonyl groups of aldehyde monomers.[43] Hence, the morphology evolution behaviors of TpPa can be well regulated. Because the formation of TpPa followed a nucleation-growth process, monomers with high reactivity would be rapidly converted into prepolymers (that is, oligomers and crystal nuclei) so that they could be further ripened into highly crystalline TpPa according to dynamic chemistry.[44,45] When the pH value was 1.8, pronounced protonation of amino groups inside prepolymers occurred, resulting in a significantly inhibited prepolymer ripening process. Under the influence of the encapsulation of surfactants and retarded ripening process, the prepolymers were prone to grow into nanofibers along one dimension rather than the entire two-dimensional plane (Fig. 6). Because the growth was confined in one dimension, consequently, as the synthesis duration was extended to 72 h, the short fibers evolved into long fibers which was driven by the noncovalent forces among the COF interlayers.[46] This can be proven by time-dependent SEM imaging analysis. In contrast, when the pH value was 2.5, amino groups inside the prepolymers exhibited moderate protonation. The ripening process was not largely inhibited as earlier, and in-plane growth (that is, along the two-dimensional plane) occurred with the assistance of surfactants. Thus, initially, alongside the short fibers, small plates reasonably emerged, as demonstrated previously. Moreover, moderate protonation favored the assembly and fusion of short fibers in two dimensions instead of propagating in one dimension, eventually giving rise to the formation of plates (Fig. 6). This result can account for the relatively low BET surface area of TpPa nanoplates. The main reason is that the morphology evolution inevitably influenced the BET surface area. In

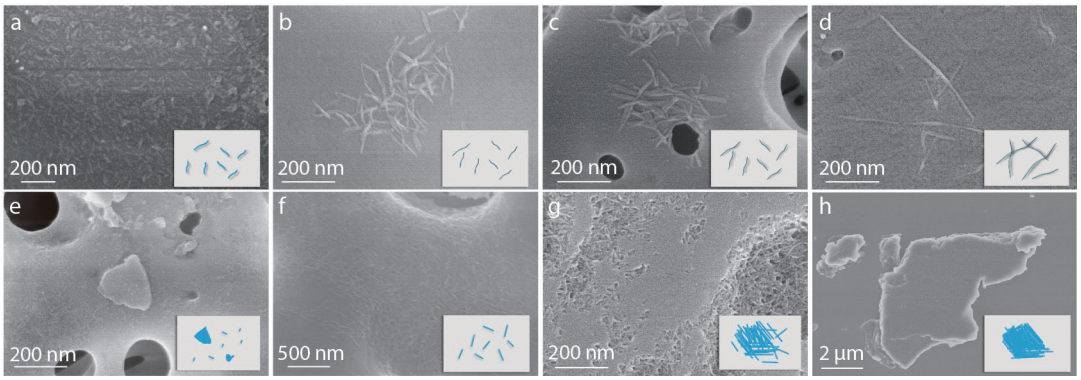


**Fig. 4** SEM images of TpPa nanofibers and nanoplates formed at different synthesis durations. TpPa nanofibers formed at 0 h (a), 0.5 h (b), 1 h (c), and 72 h (d). TpPa nanoplates formed at 0 h (e), 0.5 h (f), 1 h (g), and 72 h (h). Insets are schematic diagrams of the corresponding TpPa morphologies.

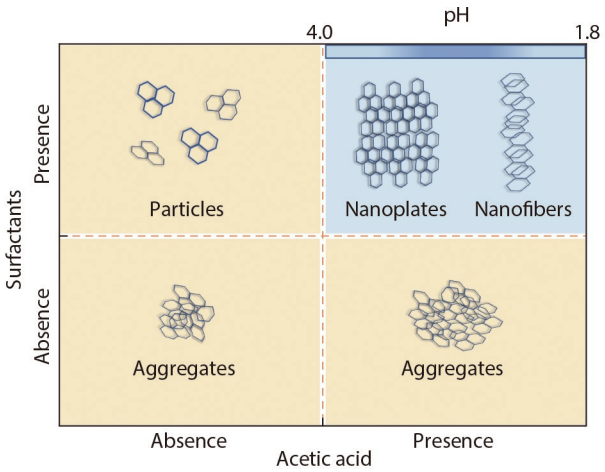


**Fig. 5** Schematic diagram of the morphology formation of TpPa by surfactant mediation and acetic acid adjustment.

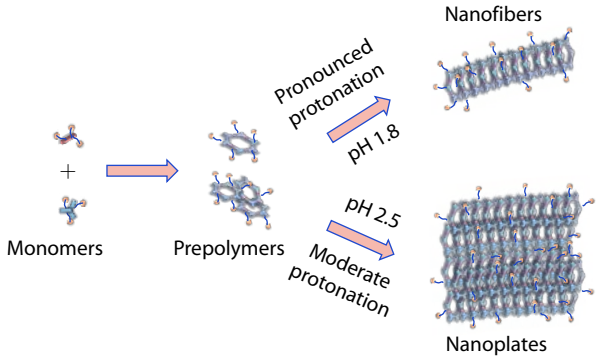


**Fig. 6** Schematic diagram of the morphology evolution of TpPa by surfactant mediation and acetic acid adjustment.

particular, the nanofibers were assembled along the one dimension, while the nanoplates were produced by assembling and fusing of the nanofibers along the two dimension. Therefore, the nanopores could be partially blocked by the assembly and fusion of nanofibers, compromising the nanoporosity of nanoplates to some extent. Overall, the morphology formation and evolution of TpPa can be described as the synergistic enhancement of surfactant mediation and acid adjustment. In addition, TpPa nanofibers possess high crystallinity and a large surface area, making them very promising in the fabrication of high-performance separation membranes, which will be presented in future work.

## CONCLUSIONS

In summary, we have developed a strategy of surfactant mediation coupled with acid adjustment to controllably engineer the morphology formation and evolution of TpPa. The surfactants can encapsulate the monomers and prepolymers to form micelles, thus creating well-defined nanostructures with either nanofibers or nanoplates. Moreover, acetic acid played an important role in the formation and evolution of nanofibers and nanoplates, as the amino groups inside the prepolymers can be protonated precisely, enabling control over the reaction process by slowing their ripening processes. Therefore, nanofibers and nanoplates can be effectively formed and continuously evolved by the synergistic enhancement of surfactant mediation and acid adjustment. TpPa nanofibers exhibited a high length-diameter ratio with a diameter down to ~20 nm and a length of up to a few microns. However, TpPa nanoplates possessed a thickness of ~18 nm. This work elucidated the mechanism underlying the morphology formation and evolution of TpPa, which is expected to pave the way to precisely control the growth of COFs and may find significant applications in diverse fields.

## NOTES

The authors declare no competing financial interest.

## Electronic Supplementary Information

Electronic supplementary information (ESI) is available free of charge in the online version of this article at http://doi.org/10.1007/s10118-022-2676-6.

## ACKNOWLEDGMENTS

This work was financially supported by the National Natural Science Foundation of China (No. 21921006).

## REFERENCES

1 Wang, Z. F.; Zhang, S. N.; Chen, Y.; Zhang, Z. J.; Ma, S. Q. Covalent organic frameworks for separation applications. *Chem. Soc. Rev.* **2020**, *49*, 708–735.
2 Zhao, X. J.; Pachfule, P.; Thomas, A. Covalent organic frameworks (COFs) for electrochemical applications. *Chem. Soc. Rev.* **2021**, *50*, 6871–6913.
3 Esrafili, A.; Wagner, A.; Inamdar, S.; Acharya, A. P. Covalent organic frameworks for biomedical applications. *Adv. Healthc. Mater.* **2021**, *10*, 2002090.
4 Zhu, D.; Xu, G.; Barnes, M.; Li, Y.; Tseng, C. P.; Zhang, Z.; Zhang, J. J.; Zhu, Y.; Khalil, S.; Rahman, M. M.; Verduzco, R.; Ajayan, P. M. Covalent organic frameworks for batteries. *Adv. Funct. Mater.* **2021**, *31*, 2100505.
5 Iqbal, R.; Badshah, A.; Ma, Y. J.; Zhi, L. J. An electrochemically stable 2D covalent organic framework for high-performance organic supercapacitors. *Chinese J. Polym. Sci.* **2020**, *38*, 558–564.
6 Gropp, C.; Canossa, S.; Wuttke, S.; Gandara, F.; Li, Q.; Gagliardi, L.; Yaghi, O. M. Standard practices of reticular chemistry. *ACS Cent. Sci.* **2020**, *6*, 1255–1273.
7 Sun, D. W.; Huang, L. J.; Pu, H. B.; Ma, J. Introducing reticular chemistry into agrochemistry. *Chem. Soc. Rev.* **2021**, *50*, 1070–1110.
8 Zhu, Y.; Shao, P.; Hu, L.; Sun, C.; Li, J.; Feng, X.; Wang, B. Construction of interlayer conjugated links in 2D covalent organic frameworks *via* topological polymerization. *J. Am. Chem. Soc.* **2021**, *143*, 7897–7902.
9 Haase, F.; Lotsch, B. V. Solving the COF trilemma: towards crystalline, stable and functional covalent organic frameworks. *Chem. Soc. Rev.* **2020**, *49*, 8469–8500.
10 Kandambeth, S.; Dey, K.; Banerjee, R. Covalent organic frameworks: chemistry beyond the structure. *J. Am. Chem. Soc.* **2019**, *141*, 1807–1822.
11 Smith, B. J.; Overholts, A. C.; Hwang, N.; Dichtel, W. R. Insight into the crystallization of amorphous imine-linked polymer networks to 2D covalent organic frameworks. *Chem. Commun.* **2016**, *52*, 3690–3693.
12 Huang, W.; Jiang, Y.; Li, X.; Li, X. J.; Wang, J. Y.; Wu, Q.; Liu, X. K. Solvothermal synthesis of microporous, crystalline covalent organic framework nanofibers and their colorimetric nanohybrid

structures. *ACS Appl. Mater. Interfaces* **2013**, *5*, 8845–8854.
13 Guan, Q.; Wang, G. B.; Zhou, L. L.; Li, W. Y.; Dong, Y. B. Nanoscale covalent organic frameworks as theranostic platforms for oncotherapy: synthesis, functionalization, and applications. *Nanoscale Adv.* **2020**, *2*, 3656–3733.
14 Tao, S.; Xu, H.; Xu, Q.; Hijikata, Y.; Jiang, Q.; Irle, S.; Jiang, D. Hydroxide anion transport in covalent organic frameworks. *J. Am. Chem. Soc.* **2021**, *143*, 8970–8975.
15 Geng, K.; He, T.; Liu, R.; Dalapati, S.; Tan, K. T.; Li, Z.; Tao, S.; Gong, Y.; Jiang, Q.; Jiang, D. Covalent organic frameworks: design, synthesis, and functions. *Chem. Rev.* **2020**, *120*, 8814–8933.
16 Liu, R.; Tan, K. T.; Gong, Y.; Chen, Y.; Li, Z.; Xie, S.; He, T.; Lu, Z.; Yang, H.; Jiang, D. Covalent organic frameworks: an ideal platform for designing ordered materials and advanced applications. *Chem. Soc. Rev.* **2021**, *50*, 120–242.
17 Liu, W.; Li, X.; Wang, C.; Pan, H.; Liu, W.; Wang, K.; Zeng, Q.; Wang, R.; Jiang, J. A scalable general synthetic approach toward ultrathin imine-linked two-dimensional covalent organic framework nanosheets for photocatalytic $CO_2$ reduction. *J. Am. Chem. Soc.* **2019**, *141*, 17431–17440.
18 Zhao, W.; Wang, T. P.; Wu, J. L.; Pan, R. P.; Liu, X. Y.; Liu, X. K. Monolithic covalent organic framework aerogels through framework crystallization induced self-assembly: heading towards framework materials synthesis over all length scales. *Chinese J. Polym. Sci.* **2019**, *37*, 1045–1052.
19 Das, G.; Benyettou, F.; Sharma, S. K.; Sharama, S. K.; Prakasam, T.; Gandara, F.; de la Pena-O'Shea, V. A.; Saleh, N.; Pasricha, R.; Jagannathan, R.; Olson, M. A.; Olson, A. Covalent organic nanosheets for bioimaging. *Chem. Sci.* **2018**, *9*, 8382–8387.
20 Peng, Y.; Huang, Y.; Zhu, Y.; Chen, B.; Wang, L.; Lai, Z.; Zhang, Z.; Zhao, M.; Tan, C.; Yang, N.; Shao, F.; Han, Y.; Zhang, H. Ultrathin two-dimensional covalent organic framework nanosheets: preparation and application in highly sensitive and selective DNA detection. *J. Am. Chem. Soc.* **2017**, *139*, 8698–8704.
21 Liu, Y. Y.; Li, X. C.; Wang, S.; Cheng, T.; Yang, H.; Liu, C.; Gong, Y.; Lai, W. Y.; Huang, W. Self-templated synthesis of uniform hollow spheres based on highly conjugated three-dimensional covalent organic frameworks. *Nat. Commun.* **2020**, *11*, 5561.
22 Wang, Y.; Xie, M.; Lan, J.; Yuan, L.; Yu, J.; Li, J.; Peng, J.; Chai, Z.; Gibson, J. K.; Zhai, M.; Shi, W. Radiation controllable synthesis of robust covalent organic framework conjugates for efficient dynamic column extraction of $^{99}TcO_4^-$. *Chem* **2020**, *6*, 2796–2809.
23 Gole, B.; Stepanenko, V.; Rager, S.; Grüne, M.; Medina, D. D.; Bein, T.; Würthner, F.; Beuerle, F. Microtubular self-assembly of covalent organic frameworks. *Angew. Chem. Int. Ed.* **2018**, *57*, 846–850.
24 Zhang, Z.; Shi, X. S.; Wang, R.; Xiao, A.; Wang, Y. Ultra-permeable polyamide membranes harvested by covalent organic framework nanofiber scaffolds: a two-in-one strategy. *Chem. Sci.* **2019**, *10*, 9077–9083.
25 Sun, Q.; Aguila, B.; Perman, J.; Earl, L. D.; Abney, C. W.; Cheng, Y.; Wei, H.; Nguyen, N.; Wojtas, L.; Ma, S. Postsynthetically modified covalent organic frameworks for efficient and effective mercury removal. *J. Am. Chem. Soc.* **2017**, *139*, 2786–2793.
26 Zhang, F.; Zhang, J.; Zhang, B.; Tan, X.; Shao, D.; Shi, J.; Tan, D.; Liu, L.; Feng, J.; Han, B.; Yang, G.; Zheng, L.; Zhang, J. Room-temperature synthesis of covalent organic framework (COF-LZU1) nanobars in $CO_2$/water solvent. *ChemSusChem* **2018**, *11*, 3576–3580.
27 Yamada, H.; Urata, C.; Higashitamori, S.; Aoyama, Y.; Yamauchi, Y.; Kuroda, K. Critical roles of cationic surfactants in the preparation of colloidal mesostructured silica nanoparticles: control of mesostructure, particle size, and dispersion. *ACS Appl. Mater. Interfaces* **2014**, *6*, 3491–3500.
28 Yang, H.; Coombs, N.; Ozin, G. A. Morphogenesis of shapes and surface patterns in mesoporous silica. *Nature* **1997**, *386*, 692–695.
29 Li, K.; Lin, S.; Li, Y.; Zhuang, Q.; Gu, J. Aqueous-phase synthesis of mesoporous Zr-based MOFs templated by amphoteric surfactants. *Angew. Chem. Int. Ed.* **2018**, *57*, 3439–3443.
30 Alizadeh, S.; Nematollahi, D. Electrochemically assisted self-assembly technique for the fabrication of mesoporous metal-organic framework thin films: composition of 3D hexagonally packed crystals with 2D honeycomb-like mesopores. *J. Am. Chem. Soc.* **2017**, *139*, 4753–4761.
31 Zhang, S.; Wu, X.; Ma, C.; Li, Y.; You, J. Cationic surfactant modified 3D COF and its application in the adsorption of UV filters and alkylphenols from food packaging material migrants. *J. Agric. Food Chem.* **2020**, *68*, 3663–3669.
32 Sahabudeen, H.; Qi, H.; Ballabio, M.; Polozij, M.; Olthof, S.; Shivhare, R.; Jing, Y.; Park, S.; Liu, K.; Zhang, T.; Ma, J.; Rellinghaus, B.; Mannsfeld, S.; Heine, T.; Bonn, M.; Canovas, E.; Zheng, Z.; Kaiser, U.; Dong, R.; Feng, X. Highly crystalline and semiconducting imine-based two-dimensional polymers enabled by interfacial synthesis. *Angew. Chem. Int. Ed.* **2020**, *59*, 6028–6036.
33 Poyraz, A. S.; Albayrak, C.; Dag, Ö. The effect of cationic surfactant and some organic/inorganic additives on the morphology of mesostructured silica templated by pluronics. *Microporous Mesoporous Mater.* **2008**, *115*, 548–555.
34 Liang, Y.; Zhu, Y.; Liu, C.; Lee, K. R.; Hung, W. S.; Wang, Z.; Li, Y.; Elimelech, M.; Jin, J.; Lin, S. Polyamide nanofiltration membrane with highly uniform sub-nanometre pores for sub-1 A precision separation. *Nat. Commun.* **2020**, *11*, 2015.
35 Franco, C.; Rodriguez-San-Miguel, D.; Sorrenti, A.; Sevim, S.; Pons, R.; Platero-Prats, A. E.; Pavlovic, M.; Szilagyi, I.; Ruiz Gonzalez, M. L.; Gonzalez-Calbet, J. M.; Bochicchio, D.; Pesce, L.; Pavan, G. M.; Imaz, I.; Cano-Sarabia, M.; Maspoch, D.; Pane, S.; de Mello, A. J.; Zamora, F.; Puigmarti-Luis, J. Biomimetic synthesis of sub-20 nm covalent organic frameworks in water. *J. Am. Chem. Soc.* **2020**, *142*, 3540–3547.
36 Kandambeth, S.; Mallick, A.; Lukose, B. V.; Mane, M.; Heine, T.; Banerjee, R. Construction of crystalline 2D covalent organic frameworks with remarkable chemical (acid/base) stability *via* a combined reversible and irreversible route. *J. Am. Chem. Soc.* **2012**, *134*, 19524–19527.
37 Kong, D. Y.; Chen, Z. L. Covalent organic framework TpPa-1 as stationary phase for capillary electrochromatographic separation of drugs and food additives. *Electrophoresis* **2018**, *39*, 2912–2918.
38 Li, Y.; Pei, B.; Chen, J.; Bing, S.; Hou, L.; Sun, Q.; Xu, G.; Yao, Z.; Zhang, L. Hollow nanosphere construction of covalent organic frameworks for catalysis: (Pd/C)@TpPa COFs in Suzuki coupling reaction. *J. Colloid Interface Sci.* **2021**, *591*, 273–280.
39 Pérez-Carvajal, J.; Boix, G.; Imaz, I.; Maspoch, D. The Imine-based COF TpPa-1 as an efficient cooling adsorbent that can be regenerated by heat or light. *Adv. Energy Mater.* **2019**, *9*, 1901535.
40 Shi, X. S.; Ma, D. W.; Xu, F.; Zhang, Z.; Wang, Y. Table-salt enabled interface-confined synthesis of covalent organic framework (COF) nanosheets. *Chem. Sci.* **2019**, *11*, 989–996.
41 Hu, X.; Jian, J.; Fang, Z.; Zhong, L.; Yuan, Z.; Yang, M.; Ren, S.; Zhang, Q.; Chen, X.; Yu, D. Hierarchical assemblies of conjugated ultrathin COF nanosheets for high-sulfur-loading and long-lifespan lithium-sulfur batteries: fully-exposed porphyrin matters. *Energy Storage Mater.* **2019**, *22*, 40–47.
42 Tan, J.; Namuangruk, S.; Kong, W.; Kungwan, N.; Guo, J.; Wang, C. Manipulation of amorphous-to-crystalline transformation: towards the construction of covalent organic framework hybrid microspheres with NIR photothermal conversion ability. *Angew. Chem. Int. Ed.* **2016**, *55*, 13979–13984.
43 Martin-Illan, J. A.; Rodriguez-San-Miguel, D.; Franco, C.; Imaz, I.; Maspoch, D.; Puigmarti-Luis, J.; Zamora, F. Green synthesis of imine-based covalent organic frameworks in water. *Chem. Commun.* **2020**, *56*, 6704–6707.
44 Sasmal, H. S.; Halder, A.; Kunjattu H, S.; Dey, K.; Nadol, A.; Ajithkumar, T. G.; Bedadur, P. R.; Banerjee, R. Covalent self-assembly in two dimensions: connecting covalent organic framework nanospheres into crystalline and porous thin films. *J. Am. Chem. Soc.* **2019**, *141*, 20371–20379.
45 Nguyen, H. L.; Gropp, C.; Yaghi, O. M. Reticulating 1D ribbons into 2D covalent organic frameworks by imine and imide linkages. *J. Am. Chem. Soc.* **2020**, *142*, 2771–2776.
46 Dong, W. L.; Li, S. Y.; Yue, J. Y.; Wang, C.; Wang, D.; Wan, L. J. Fabrication of bilayer tetrathiafulvalene integrated surface covalent organic frameworks. *Phys. Chem. Chem. Phys.* **2016**, *18*, 17356–17359.

https://doi.org/10.1007/s10118-022-2676-6